RESEARCH ARTICLE

Macromolecular Rapid Communications
www.mrc-journal.de

Real and In Silico Microgels Show Comparable Bulk Moduli Below and Above the Volume Phase Transition

*Tom Höfken, Urs Gasser, Stefanie Schneider, Alexander V. Petrunin, and Andrea Scotti**

The compressibility of soft colloids influences their phase behavior and flow properties, especially in concentrated suspensions. Particle compressibility, which is proportional to the reciprocal of the bulk modulus *K*, is a key parameter for soft polymer-based particles that can be compressed in crowded environments. Here, microgels with different degrees of cross-linking, i.e., softness, are investigated below and above their volume phase transition temperature (VPTT). By combining molecular dynamics simulations with small-angle neutron scattering with contrast variation, a change in the particle bulk moduli of two orders of magnitude is observed. The degree of cross-linking has a significant impact on the bulk modulus of the swollen microgel, while above the VPTT the values of *K* are almost independent of the cross-linking density. The excellent agreement between experimental results and simulations also highlight that the model microgels from computer simulations possess both the internal architecture and the elastic properties of real polymeric networks. This paves the way to a systematic use of simulations to investigate the behavior of dense microgel suspensions below and above their VPTT.

1. Introduction

Microgels, cross-linked polymer networks swollen in a good solvent, are a commonly studied model-system for soft colloids.[1–3] When synthesized starting from a monomer with a lower critical solution temperature (LCST), they exhibit responsiveness to external stimuli. This property makes microgels interesting for various applications such as a stabilizer to obtain smart emulsions that can be broken on demand simply by changing the temperature.[4–6] Microgel thermoresponsiveness is also pivotal in the use of these materials as drug or gene delivery systems.[1,7] Moreover, investigating microgels provides valuable insights into the impact of softness on phase transitions and flow properties.[3]

The most prominent example of thermoresponsive microgels is the one synthesized using poly(*N*-isopropylmethacylamide) (pNIPAM).[2] An increase in temperature reduces the quality of water as a solvent, so that it is expelled from the particle.[8] This enables the on-demand change of packing fraction by simply adjusting the temperature, allowing, for instance, to study the crystallization of soft spheres at different packing fractions,[9–11] the glass-to-jamming transition,[12–14] and the flow behavior of complex fluids.[15,16] Consequently, the prediction of microgel properties using computer simulations, in silico, holds significant appeal and is already a common procedure.[17–19] For dense systems, one of the most important properties a model microgel must reproduce is the particle bulk modulus *K*, which is proportional to the inverse of the particle compressibility, since this modulus plays a key role in determining the microgel response to isotropic compression.[20–22]

For large microgels ($\geqslant$ 1 μm), *K* is accessible experimentally by combining osmotic stress polymers with microscopy[23,24] or using capillary micromechanics and microfluidics.[25] However, for many applications and fundamental studies, it is desirable to have microgels with radii smaller than a few hundreds of nanometers,[3,26] rendering these tools unusable. Furthermore, large microgels may not serve as ideal comparisons for theoretical results since simulations are often constrained to smaller systems.[18] Recently, we developed a method based on osmotic stress exerted by deuterated polymer that uses small-angle neutron scattering (SANS) with contrast variation to determine the value of the bulk modulus experimentally and its evolution upon compression for soft compressible colloids with

T. Höfken, S. Schneider, A. V. Petrunin
Institute of Physical Chemistry
RWTH Aachen University
Landoltweg 2, 52074 Aachen, Germany
U. Gasser
Laboratory for Neutron Scattering and Imaging
Paul Scherrer Institut
Villigen 5232, Switzerland
A. Scotti
Department of Biomedical Science, Faculty of Health and Society
Malmö University
Malmö SE-205 06, Sweden
E-mail: andrea.scotti@mau.se
A. Scotti
Biofilms—Research Center for Biointerfaces
Malmö University
Malmö SE-205 06, Sweden

The ORCID identification number(s) for the author(s) of this article can be found under https://doi.org/10.1002/marc.202400043

DOI: 10.1002/marc.202400043

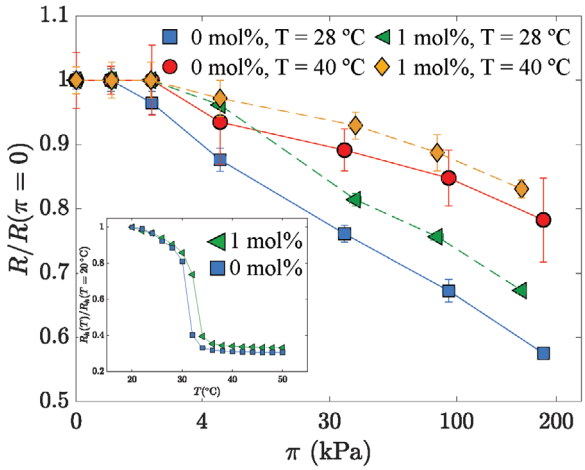

Figure 1. Normalized radii as determined by SANS normalized vs osmotic pressure. Inset: normalized hydrodynamic radii as a function of temperature.

dimensions of a few hundred nanometers.[27,28] From a computational perspective, the bulk modulus can be determined from molecular dynamics simulations of a bead-spring microgel by calculating the dependency of the microgel volume on the pressure and extracting the bulk modulus from the slope of the linear regime at low pressure and volume,[29] or by considering volume fluctuations.[30]

Here, we extend our previous study[27] and determine the evolution of the bulk modulus of pNIPAM microgels cross-linked with N,N'-methylenebisacrylamide (BIS) at different temperature and swelling degrees, below and above their volume phase transition temperature (VPTT). Without changing solvent quality, the softness of microgels is mainly influenced by the amount of cross-linker used during the synthesis.[27] In contrast, the values of K for microgels above their VPTT are identical, within the experimental error, independent of the amount of cross-linker used during the synthesis. These experimental results are then compared with the values of K obtained for in silico microgels revealing a quantitative agreement in both their absolute values and evolution through the volume phase transition.

2. Results and Discussion

2.1. Small-Angle Neutron Scattering

The inset of **Figure 1** shows the swelling curves for the two microgels studied. The hydrodynamic radii R_h of dilute solutions of microgels ($c \lesssim 0.1$ wt%) have been determined using multi-angle dynamic light scattering. The values of R_h of the microgels are normalized to the values of R_h at a temperature $T = 20$ °C and plotted as a function of T. The particles were synthesized via precipitation polymerization using 1 mol% (squares) and 0 mol% (circles) of additional cross-linker, see Supporting Information for further information. The 0% crosslinked particles are known as ultra-low cross-linked (ULC) microgels, and their polymeric network is formed due to the hydrogen atom abstraction at the tertiary carbon atom of the isopropyl group.[31] For both microgels, a dramatic change in size happens at $T \simeq 32$ °C. From the literature it is known that the VPTT shifts to slightly larger T with increasing the amount of BIS during the synthesis,[15,32] and this is the case even when only 1 mol% BIS is added, as shown by the triangles in the inset of Figure 1. The ratio between the radius in the swollen state, at $T = 20$ °C, and in the collapsed state gives us a first idea on the microgel's softness; larger values of this ratio, $S_D = R_h(20\,°C)/R_h(40\,°C)$, correspond to softer microgels.[3] The values of S_D are 3.01 ± 0.02 and 3.29 ± 0.03 for the 1 mol% crosslinked and the ULC microgels, respectively. This shows that the ULC microgels are slightly softer.

However, defining the softness of microgels solely based on the swelling ratio can be misleading, since it ignores other particle's characteristics that can affect the microgel compressibility. Additional parameters, such as the degree of interpenetration, the extent of deformation and faceting, and the deformability upon adsorption must be taken into account to accurately quantify the softness of an object.[3] For instance, microgel ability to deswell due to external stimuli, such as temperature, is not necessarily coupled to their behavior at increasing osmotic pressure. Changes in the swelling state of the microgel in turn influence their bulk modulus since the more a microgel is compressed, the harder it becomes to compress it further.[27,33] Therefore, a more complete quantification of the particle softness can be given by measuring its bulk modulus, $K = -\nu\frac{d\pi}{d\nu}$, where π is the osmotic stress and ν is the particle volume. Furthermore, a single value of K is not sufficient to describe the particle softness since, in contrast to hard particles, for compressible colloids the value of K evolves with particle compression or with deswelling caused by external stimuli, underlining the need of multiple parameters to quantify softness.[27,28]

To probe the value and the evolution of K for the microgels studied here, a high molecular weight ($M_n = 265000$ g mol^{-1}) partially deuterated polymer, polyethylene glycol (PEG), has been synthesized. The deuterated PEG used here is the same used previously and has a degree of deuteration of 83% ($d_{83\%}PEG$).[27,28] Given the high value of M_n the polymer cannot penetrate the particle and we have shown that its only effect, even at high concentration, is to increase the osmotic pressure leading to an isotropic deswelling.[27,28] When used for small-angle neutron scattering (SANS), the scattering length density (SLD) of $d_{83\%}PEG$ is the same as the one of heavy water (D_2O), i.e., the polymer is contrast matched. This means that we can increase $d_{83\%}PEG$ concentration, and consequently the osmotic stress experienced by the microgels, to unprecedentedly high values but the polymer does not contribute to the measured coherent intensity, $I(q)$. Therefore, once the concentration of microgels in solution is low enough, such that the structure factor of the particles is one, $I(q)$ is proportional to the particle form factor of the microgels $P(q)$. The analysis of these data allows us to experimentally probe the variation of the characteristic lengths of the microgels (e.g., total size, extension of the fuzzy shell) at different π.

Figure 2a,b shows the form factors of the microgels synthesized with 1 mol% cross-linker measured at 28 (left side triangles) and 42°C (diamonds), respectively. The microgel concentration is kept constant and in all samples, they occupy less than 8% of the available volume. In contrast, the concentration of $d_{83\%}PEG$ increases from zero (bottom curve) up to 7.44 ± 0.01 wt%. The mass concentrations in weight percent, c, are then converted into osmotic stress, π, using an empiric relation measured for the used

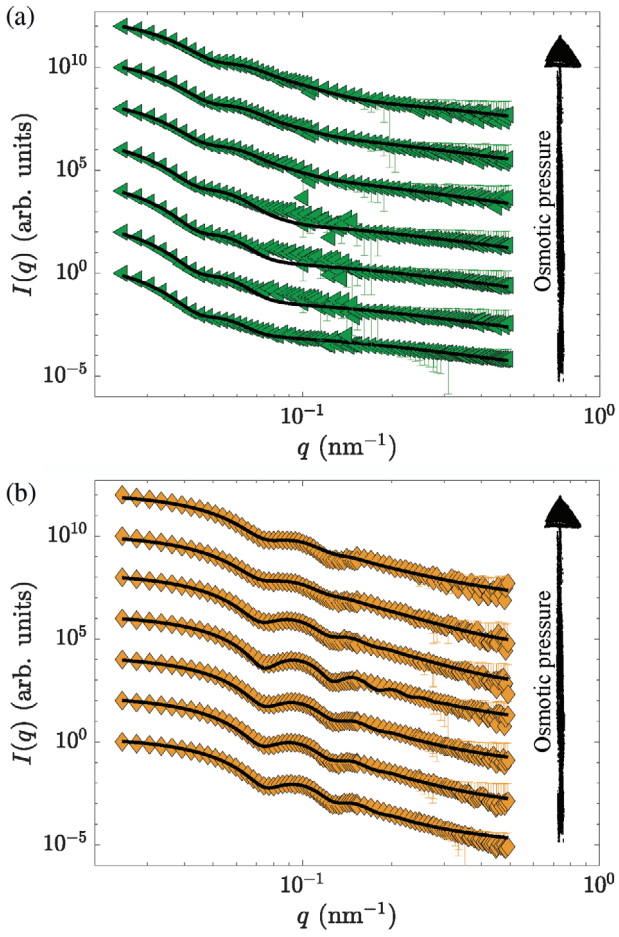

Figure 2. Small-angle neutron scattering intensities vs. scattering vector for the 1 mol% cross-linked microgels at 28°C (a) and 42 °C (b). The applied osmotic stress increases from bottom (0 kPa) to top (≈160 kPa). Solid lines are data fits with the fuzzy-sphere model.[34]

polymer[27]: $\pi = 217$ Pa $c + 451$ Pa c^3. The curves in Figure 2 are measured between $\pi = 0$ (bottom) and $\pi \simeq 160$ kPa.

For both temperatures measured, the first oscillation in the particles form factors moves to higher values of q with increasing osmotic stress: for the triangles (28 °C) it goes from 2.6 × 10^{-2} nm^{-1} (bottom) to 4 × 10^{-2} nm^{-1} (top) while for the diamonds (42 °C) it moves from 6.4 × 10^{-2} nm^{-1} to 7.1 × 10^{-2} nm^{-1}. This behavior corresponds to a change in the characteristic lengths scales of the particles. To quantify these changes, the data are fitted with a well established model for a fuzzy-sphere[34] which has been proven to well reproduce the form factors of both cross-linked[34–37] and ultra-low cross-linked[38–40] below and above the VPTT.

The solid lines in Figure 2 represent the fits using the fuzzy-sphere model. The total radius of the microgel, R, the radius of the more homogeneous core, R_c, the length of the fuzzy shell, 2σ, the mesh size of the polymeric network, ξ, and the percentage of size polydispersity, p, are the structural parameters obtained from the fits. We note that in the middle q-range the accuracy of some fit is not completely satisfactory (solid line and left-side triangles). This can be due to the fact that in this region we merge two different set of data measured at different sample-detector distances and, consequently, q-resolution.

In Figure 1, the variation of the total radius of the particles, normalized to the values determined when no pressure is applied, are plotted as a function of the increasing osmotic stress. The triangles and diamonds represent the evolution of the radius for the 1 mol% cross-linked microgels at 28 °C and 42 °C, respectively. In the same figure, the squares and circles represent the values of the radius of the ULC microgels at 28 °C and 42 °C, respectively. These data are obtained from the fits of the form factors of ULC microgels at different osmotic stress shown in Figure S1 (Supporting Information). As can be seen, a clear decrease of the microgel size is observed for all microgels at all temperatures with increasing π.

The values of the radii R in Figure 1 are then used to compute the microgel volume at different compression $v = \frac{4}{3}\pi R^3$ and the data are plotted in a π vs v representation (**Figure 3a**). This particular choice is related to the fact that the point-to-point slopes of the curves in Figure 3a are proportional to the microgel bulk moduli. Therefore, for every couple of adjacent points, i and $i+1$, the bulk modulus is computed as $K_i = -v\frac{\pi_{i+1}-\pi_i}{v_{i+1}-v_i}$. It must be considered that the differences between volumes in the denominator are of the order of 10^{-22} m^3. Therefore, errors on the volumes of the same order of magnitude will lead to considerable errors on the value of K_i. Values of K_i with an error larger than 20% are ignored.

Figure 3b shows the obtained values of K for the 1 mol% cross-linked microgels at 28 °C (left side triangles) and 42 °C (diamonds), and for the ULC microgels at 28 °C (squares) and 42 °C (circles). The degree of compression is given by the quantity $1 - v/v_0$, where at the fixed temperature T, v and v_0 are the microgel volumes at a given compression and in the uncompressed state, respectively. Zero compression corresponds to $1 - v/v_0 = 0$, while higher values reflect a higher compression. In the same panel, the values of the bulk moduli at 20 °C, i.e., in the swollen state, as determined in our previous study[27] are reported as upright triangles and stars for the 1 mol% and the ULC microgels, respectively.

As can be seen in Figure 3b, the value of K increases with increasing the particle compression for all the temperature. At 28 °C (left side triangles), the first value of K determined for the 1 mol% cross-linked microgels is 87 kPa that increases with compressing the microgels up to 252 kPa for the highest osmotic stress measured. At 42 °C (diamonds), initially $K = 274$ kPa and increases to $K = 416$ kPa. Just below the volume phase transition, at 28 °C, the bulk modulus of the ULC microgels is $K = 19$ kPa (squares). At the highest π applied, the measured values of K for the ULC microgels is 246 kPa. When the ULC are collapsed at 42 °C, their initial bulk modulus is 223 kPa that increases with compression up to 431 kPa.

Comparing the upright triangles with the diamonds (1 mol% cross-linked) and the stars with the circles (ULC) at low compression, the first result is that the stiffness of the microgels increases by two orders of magnitude when they collapse above the VPTT. The second observation is that, even when collapsed, the microgels can be further compressed with increasing osmotic pressure. This is consistent with the fact that a significant amount of water is still present in the microgels even above the VPTT.[34,35,39,41,42] It is also evident that with increasing the

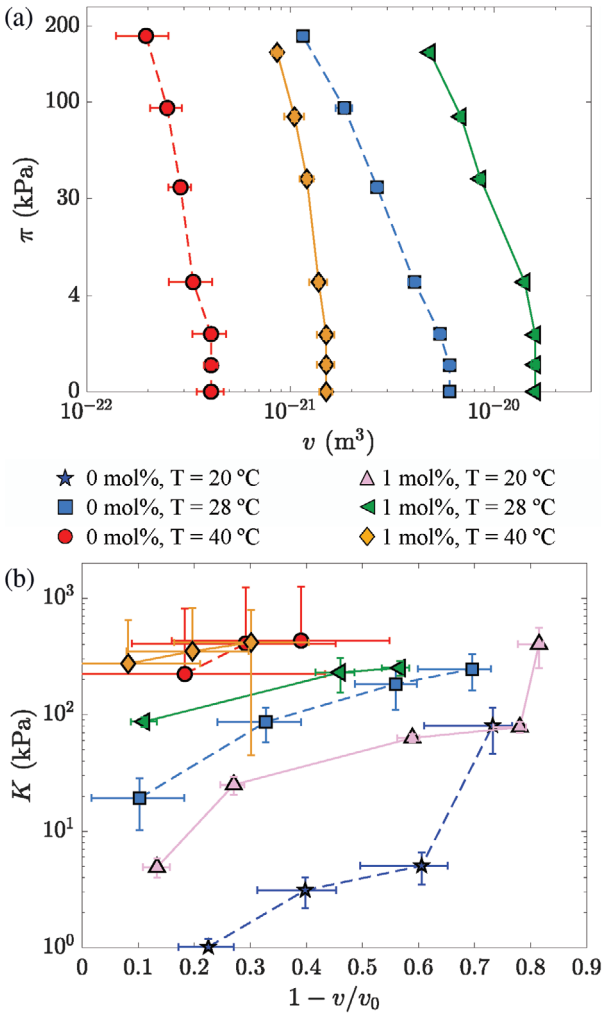

Figure 3. a) Osmotic stress π vs. changes in volume for 1 mol% cross-linked microgels at 28 °C (left-side triangles), and 42 °C (diamonds); and for ULC microgels at 28 °C (squares), and 42 °C (circles). b) Variation of the microgel bulk moduli K as a function of compression for 1 mol% cross-linked microgels at 20 °C (up-side triangles), 28 °C (left-side triangles), and 42 °C (diamonds); and for ULC microgels at 20 °C (stars), 28 °C (squares), and 42 °C (circles).

temperature the difference in softness between the ULC and 1 mol% cross-linked microgels decreases. At 20 °C, the values of the bulk modulus of the ULC (stars) remains smaller than the ones of the 1 mol% crosslinked microgels up to $1–v/v_0 \approx 0.75$. This difference is reduced at 28 °C and disappear for $1–v/v_0 \approx 0.55$ (squares and left-side triangle). Finally, well above the microgel VPTT, at 40 °C, both the ULC (circles) and the 1 mol% cross-linked microgels (diamonds) have, within the experimental errors, the same bulk modulus.

3. Molecular Dynamics Simulation

Our molecular dynamics simulations are based on a standard bead-spring model of neutral microgels with implicit solvent.[18] In this model, three types of interactions are considered: i) an excluded volume term between all beads using the Weeks–Chandler–Anderson potential, ii) bonding interactions using a FENE (Finite Extensible Nonlinear Elastic)-bond potential, and iii) a smooth well attractive potential to model hydrophobic interactions. For microgels in the swollen state, hydrophobic interactions are neglected, i.e., we are under conditions of a good solvent. When forming the network, the monomer beads have two bonds while cross-linker beads have a connectivity of up to four. The cross-link fraction can be controlled by the proportion of cross-linker beads. For the cross-linker beads, we made a further distinction between the regular microgels cross-linked with BIS and the ULC microgels that form cross-links via the hydrogen atom abstraction mechanism.[31] BIS forms cross-links by connecting two polymer chains along their backbones and, therefore, a cross-link bead should have a total number of four monomer neighbors. In ULC microgels, the bonds are always formed between the end of a polymer chain and a polymer backbone, which is best modeled by cross-linker beads bonding to three monomer beads. To accurately reflect the excluded volume and the microgel size, a bead has a diameter of 2 nm and a single microgel consist of $\approx 10^5$ beads. Exemplary swelling curves and density distributions are shown in Figures S3 and S4 (Supporting Information).

To compute the microgel volume and the volume fluctuations, we generate a mesh enclosing the polymer beads via the alpha shape algorithm,[43] which has already been successfully applied to microgels.[19] The alpha parameter is chosen to equal ten bead diameters. This ensures the creation of a mesh without holes and avoids overestimating the microgel volume due to single stretched dangling chain ends (Figure S2, Supporting Information). The bulk modulus is then simply calculated as ref. [30]:

$$K = k_B T \frac{< V^2 > - < V >^2}{V} \quad (1)$$

where V is the microgel volume in the simulations. All data points are averaged from simulation results of four different microgels with the same cross-linker fraction.

Figure 4a shows the bulk moduli computed for swollen microgels with trifunctional cross-links (squares) or tetrafunctional cross-links (triangles) across a range of low cross-linking fractions. In both cases, the bulk modulus increases linearly with the cross-linker fraction in the investigated range. This increase depends on the connectivity of the cross-linker, with the slope of the networks with tetrafunctional cross-link beads being roughly double the slope of those with trifunctional cross-links. At low cross-linker fractions approaching 0%, both connectivities exhibit similar values of the bulk modulus. These data reflect the microgel softness in the swollen state. The estimated value of the bulk modulus of simulated microgels is 1.0 kPa for the swollen microgel containing 1 % BIS. This value is consistent with what is determined experimentally for microgels with 1 mol% cross-linker in their swollen state (2.5 kPa).[27]

The direct comparison with ULC microgels is more challenging since the exact number of cross-links formed during synthesis is not known in advance and can be determined only approximately. An estimation based on the microgel swelling ratio[44] quantifies this concentration between 0.3% and 1.0%. The value of the bulk modulus in the swollen state for the very same ULC microgels used here has been determined in the literature and

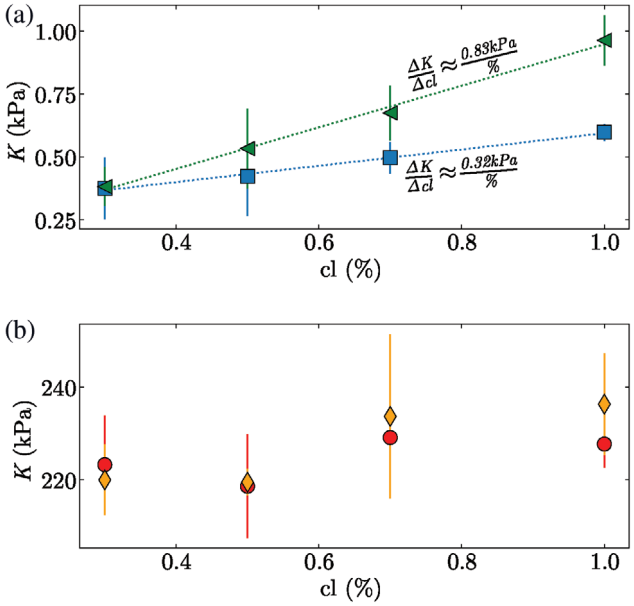

Figure 4. a) Bulk moduli of swollen microgel networks generated with different types of cross-linker beads in a regime of low cross-linking. Triangles correspond to cross-linker beads with a coordination number of four modeling the BIS cross-linker, while the squares indicate cross-linker beads with the connectivity of three that is associated with ULC microgels. b) Bulk moduli of the same microgel networks in their collapsed state for tetrafunctional cross-links (diamonds), and trifunctional cross-links (circles).

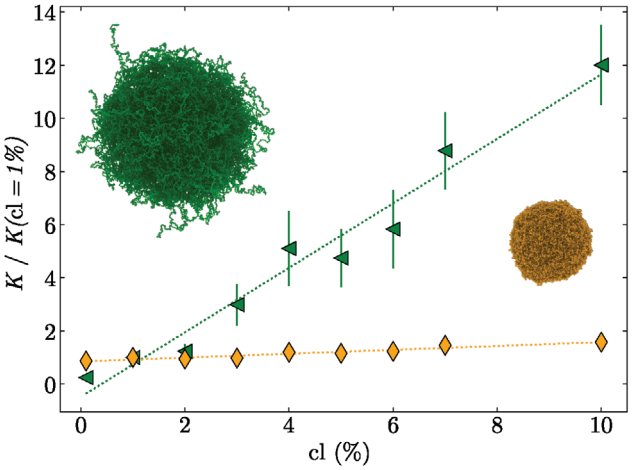

Figure 5. Relative bulk moduli of microgel networks in dependence on cross-link fraction in the swollen (green triangles) and collapsed state (orange diamonds).

equals ≃ 1 kPa in the swollen state.[27] Also this value is consistent with what we obtain from the simulations: $K_{ULC} = 0.3 - 0.5$ kPa.

Figure 4b shows the bulk moduli for the same microgels, in a collapsed state due to bad solvent conditions. Collapsing the microgel leads to an increase of the bulk modulus of about two orders of magnitude to 220–230 kPa, which is consistent with the experimental results shown by Figure 3b. When comparing the connectivity of the cross-linker bead, no trend for the bulk modulus is apparent. Similarly, the increase of cross-link concentration has little effect on the increase in the bulk modulus value in contrast to what is observed in the swollen state.

This second observation is not limited to the case of low cross-link fraction. **Figure 5** shows the values of the bulk modulus of microgels for increasing cross-linker concentrations, c_{cl}, normalized to the bulk modulus at $c_{cl} = 1\%$ for the swollen (triangles) and the collapsed state (diamonds), respectively. While the increase in the amount of cross-linker for microgels in the swollen state results in an increase of the value of the bulk modulus of an order of magnitude, the changes of the K in the collapsed state are relatively modest, with a increase of ≈1.5 from 0.3% to 10% cross-linker. The network structure of the microgel is only of secondary relevance in bad solvent, since the dominant interaction is the repulsion between solvent and polymer. In the collapsed state, polymer chains between cross-linkers are not stretched and do not contribute to the particle compressibility. This observation is reinforced by the fact that microgels with significantly different cross-link fractions exhibit similar densities in their collapsed state, as shown in Figure S4b (Supporting Information). A similar trend is observed in the experimental data, where the values of the bulk modulus of the 1 mol% cross-linked and the ULC microgels is virtually identical above the VPTT, circles and diamonds in Figure 3b.

4. Conclusion

Small-angle neutron scattering with contrast variation and molecular dynamics simulation are used here to measure the bulk moduli of microgels in the size range of hundreds of nanometers in both the swollen and the collapsed states. Experimentally, the use of neutrons is fundamental since it allows us to contrast match the partially deuterated PEG used to apply the osmotic pressure and reach unprecedentedly high values of π. In this way, in contrast to previous experiments based on dynamic light scattering,[45] we can determine both the initial values of the microgels bulk moduli and, most importantly, the evolution of K with microgel compression in proximity and above the VPTT.

Furthermore, our experimental results are mirrored by the results obtained using computer simulations. This means that the model microgels are not only structurally equivalent to the real system, e.g., they produce the same scattering profiles,[17] but have the same softness. This second aspect is fundamental for the use of this microgel model at high concentrations to better understand the properties of dense suspensions of soft colloids. The combination of both the theoretical and experimental methods can be used to systematically investigate the compressibility of microgels synthesized with different architectures, such as hollow[46] or anisotropic microgels[47] and to probe the changes of their size distribution at high concentrations.[48] Furthermore, the precise quantification of the values of K for different solvent conditions, induced by temperature, is fundamental to further develop microgels for advanced applications that rely on switching their size. For instance, when used as nanocarriers for drug delivering, the microgel softness affects their uptake into cells.[49,50] Therefore, realistic computer simulations of microgels that will help us to quantify the microgel softness and rationally design and plan their formulation for pharmaceutical application are pivotal.

Supporting Information

Supporting Information is available from the Wiley Online Library or from the author.

Acknowledgements

The authors gratefully acknowledge financial support from the Deutsche Forschungsgemeinschaft (DFG) withing the SFB 985 "Functional microgels and microgel systems". A.S. also would like to acknowledge the Knowledge Fundation (grant 20190010) for the financial support. A.S., S.S., and T.H. thank the RWTH Aachen University that granted the computation time under project rwth0946.

Conflict of Interest

The authors declare no conflict of interest.

Data Availability Statement

The data that support the findings of this study are openly available in radar4Chem at https://doi.org/[DOI:10.22000/1746], reference number 1746.

Keywords

bulk modulus, contrast variation, microgels, molecular dynamics simulations, small-angle scattering, soft colloids, soft matter

Received: January 19, 2024
Revised: April 2, 2024
Published online: May 7, 2024

[1] F. A. Plamper, W. Richtering, *Acc. Chem. Res.* **2017**, *50*, 131.
[2] M. Karg, A. Pich, T. Hellweg, T. Hoare, L. A. Lyon, J. Crassous, D. Suzuki, R. A. Gumerov, S. Schneider, I. I. Potemkin, W. Richtering, *Langmuir* **2019**, *35*, 6231.
[3] A. Scotti, M. F. Schulte, C. G. Lopez, J. J. Crassous, S. Bochenek, W. Richtering, *Chem. Rev.* **2022**, *122*, 11675.
[4] B. Brugger, S. Rütten, K.-H. Phan, M. Möller, W. Richtering, *Angew. Chem., Int. Ed.* **2009**, *48*, 3978.
[5] S. Wiese, A. C. Spiess, W. Richtering, *Angew. Chem.* **2013**, *125*, 604.
[6] W. Richtering, *Langmuir* **2012**, *28*, 17218.
[7] S. Nayak, L. A. Lyon, *Angew. Chem., Int. Ed.* **2005**, *44*, 7686.
[8] A. Scotti, U. Gasser, B. Zhou, A. Arenas-Gullo, A. de la Cotte, J. R. González, A. Fernandez-Nieves, *Smart Stimuli-Responsive Polymers, Films, and Gels*, Wiley, Hoboken, NJ **2022**, pp. 203–240.
[9] A. N. St. John, V. Breedveld, L. A. Lyon, *J. Phys. Chem. B* **2007**, *111*, 7796.
[10] J. Brijitta, B. Tata, R. Joshi, T. Kaliyappan, *J. Chem. Phys.* **2009**, *131*, 074904.
[11] H. Senff, W. Richtering, *J. Chem. Phys.* **1999**, *111*, 1705.
[12] Z. Meng, J. K. Cho, V. Breedveld, L. A. Lyon, *J. Phys. Chem. B* **2009**, *113*, 4590.
[13] D. Paloli, P. S. Mohanty, J. J. Crassous, E. Zaccarelli, P. Schurtenberger, *Soft Matter* **2013**, *9*, 3000.
[14] R. Shu, W. Sun, Y. Liu, T. Wang, C. Wang, X. Liu, Z. Tong, *Colloids Surf., A* **2013**, *436*, 912.
[15] H. Senff, W. Richtering, *Colloid Polym. Sci.* **2000**, *278*, 830.
[16] G. Chaudhary, A. Ghosh, J. G. Kang, P. V. Braun, R. H. Ewoldt, K. S. Schweizer, *J. Colloid Interface Sci.* **2021**, *601*, 886.
[17] N. Gnan, L. Rovigatti, M. Bergman, E. Zaccarelli, *Macromolecules* **2017**, *50*, 8777.
[18] L. Rovigatti, N. Gnan, L. Tavagnacco, A. J. Moreno, E. Zaccarelli, *Soft matter* **2019**, *15*, 1108.
[19] S. V. Nikolov, A. Fernandez-Nieves, A. Alexeev, *Proc. Natl. Acad. Sci.* **2020**, *117*, 27096.
[20] A. Scotti, U. Gasser, E. S. Herman, M. Pelaez-Fernandez, J. Han, A. Menzel, L. A. Lyon, A. Fernández-Nieves, *Proc. Natl. Acad. Sci. U.S.A.* **2016**, *113*, 5576.
[21] G. M. Conley, P. Aebischer, S. Nöjd, P. Schurtenberger, F. Scheffold, *Sci. Adv.* **2017**, *3*, e1700969.
[22] G. M. Conley, C. Zhang, P. Aebischer, J. L. Harden, F. Scheffold, *Nat. Commun.* **2019**, *10*, 2436.
[23] C. Gao, E. Donath, S. Moya, V. Dudnik, H. Möhwald, *Eur. Phys. J. E* **2001**, *5*, 21.
[24] V. Kozlovskaya, B. Xue, M. Dolmat, E. Kharlampieva, *Macromolecules* **2021**, *54*, 9712.
[25] P. Voudouris, D. Florea, P. van der Schoot, H. M. Wyss, *Soft Matter* **2013**, *9*, 7158.
[26] S. K. Wypysek, S. P. Centeno, T. Gronemann, D. Wöll, W. Richtering, *Macromol. Biosci.* **2023**, *23*, 2200456.
[27] J. E. Houston, L. Fruhner, A. de la Cotte, J. Rojo González, A. V. Petrunin, U. Gasser, R. Schweins, J. Allgaier, W. Richtering, A. Fernandez-Nieves, A. Scotti, *Sci. Adv.* **2022**, *8*, eabn6129.
[28] A. Scotti, U. Gasser, A. V. Petrunin, L. Fruhner, W. Richtering, J. E. Houston, *Soft Matter* **2022**, *18*, 5750.
[29] S. Nikolov, A. Fernandez-Nieves, A. Alexeev, *Appl. Math. Mech.* **2018**, *39*, 47.
[30] L. Rovigatti, N. Gnan, A. Ninarello, E. Zaccarelli, *Macromolecules* **2019**, *52*, 4895.
[31] M. Brugnoni, A. C. Nickel, L. C. Kröger, A. Scotti, A. Pich, K. Leonhard, W. Richtering, *Polym. Chem.* **2019**, *10*, 2397.
[32] T. Hellweg, C. Dewhurst, E. Brückner, K. Kratz, W. Eimer, *Colloid Polym. Sci.* **2000**, *278*, 972.
[33] P. Van Der Scheer, T. Van De Laar, J. Van Der Gucht, D. Vlassopoulos, J. Sprakel, *ACS Nano* **2017**, *11*, 6755.
[34] M. Stieger, W. Richtering, J. S. Pedersen, P. Lindner, *J. Chem. Phys.* **2004**, *120*, 6197.
[35] I. Berndt, J. S. Pedersen, W. Richtering, *J. Am. Chem. Soc.* **2005**, *127*, 9372.
[36] P. S. Mohanty, S. Nöjd, K. van Gruijthuijsen, J. J. Crassous, M. Obiols-Rabasa, R. Schweins, A. Stradner, P. Schurtenberger, *Sci. Rep.* **2017**, *7*, 1487.
[37] S. Nöjd, P. Holmqvist, N. Boon, M. Obiols-Rabasa, P. S. Mohanty, R. Schweins, P. Schurtenberger, *Soft Matter* **2018**, *14*, 4150.
[38] A. Scotti, S. Bochenek, M. Brugnoni, M.-A. Fernandez-Rodriguez, M. F. Schulte, J. Houston, A. P. Gelissen, I. I. Potemkin, L. Isa, W. Richtering, *Nat. commun.* **2019**, *10*, 1418.
[39] A. Scotti, J. Houston, M. Brugnoni, M. Schmidt, M. Schulte, S. Bochenek, R. Schweins, A. Feoktystov, A. Radulescu, W. Richtering, *Phys. Rev. E* **2020**, *102*, 052602.
[40] A. Scotti, *Soft Matter* **2021**, *17*, 5548.
[41] M. Cors, L. Wiehemeier, Y. Hertle, A. Feoktystov, F. Cousin, T. Hellweg, J. Oberdisse, *Langmuir* **2018**, *34*, 15403.
[42] M. Cors, L. Wiehemeier, O. Wrede, A. Feoktystov, F. Cousin, T. Hellweg, J. Oberdisse, *Soft matter* **2020**, *16*, 1922.
[43] H. Edelsbrunner, E. P. Mücke, *ACM Trans. Graph.* **1994**, *13*, 43.
[44] C. G. Lopez, W. Richtering, *Soft Matter* **2017**, *13*, 8271.
[45] B. Sierra-Martin, J. A. Frederick, Y. Laporte, G. Markou, J. J. Lietor-Santos, A. Fernandez-Nieves, *Colloid Polym. Sci.* **2011**, *289*, 721.
[46] A. Scotti, A. R. Denton, M. Brugnoni, J. E. Houston, R. Schweins, I. I. Potemkin, W. Richtering, *Macromolecules* **2019**, *52*, 3995.

[47] A. C. Nickel, A. Scotti, J. E. Houston, T. Ito, J. Crassous, J. S. Pedersen, W. Richtering, *Nano Lett.* **2019**, *19*, 8161.
[48] T. Höfken, C. Strauch, S. Schneider, A. Scotti, *Nano Lett.* **2022**, *22*, 2412.
[49] X. Banquy, F. Suarez, A. Argaw, J.-M. Rabanel, P. Grutter, J.-F. Bouchard, P. Hildgen, S. Giasson, *Soft Matter* **2009**, *5*, 3984.
[50] V. K. Switacz, S. K. Wypysek, R. Degen, J. J. Crassous, M. Spehr, W. Richtering, *Biomacromolecules* **2020**, *21*, 4532.